




Article

Control of Cascaded Multilevel Converter for Wave Energy Applications

Henry M. Zapata ^{1,†} , Marcelo A. Perez ^{1,†}  and Abraham Marquez Alcaide ^{2,*,†} 

¹ Department of Electronics, Universidad Tecnica Federico Santa Maria, Valparaiso 2390123, Chile

² Electronic Engineering Department, Universidad de Sevilla, 41004 Sevilla, Spain

* Correspondence: amarquez@iee.org

† These authors contributed equally to this work.

Abstract: This paper proposes a control scheme for a wave energy conversion system based on a linear generator and a cascaded multilevel converter. The mechanical conversion system is composed of a buoy connected directly to a linear generator. The windings of the generator are individually controlled by a cascaded multilevel power converter using independent maximum power point tracking to improve energy harvesting. The output of the cascaded converter is controlled to keep the DC capacitors balanced and generate a multilevel voltage at the output terminals which reduces the losses in the underwater transmission line. Experimental results show the performance of the proposed control scheme maximizing the power generation by imposing a current with the same waveform of the induced voltage and balancing the DC capacitors.

Keywords: wave energy converter; linear generator; cascaded multilevel converter

1. Introduction

Ocean energy has been increasingly developed during the last decades, motivated by its high potential, worldwide availability, and environmental concerns regarding ongoing fossil fuel utilization [1]. Considering tidal, ocean currents, waves, temperature, and salinity gradients, the global installed capacity of ocean power reached 527 MW in late 2020 [2].

The energy of waves has the most considerable harvesting potential with a global estimated power of 2 TW [3]. The wave energy resources are concentrated in areas closer to the poles, as shown in Figure 1. The coast of Chile, at the west shore of South America, particularly, offers a high mean wave power and low resource variability into the year, which are beneficial characteristics to develop this kind of renewable energy [4].

There are several initiatives promoted by the Chilean government to impulse the development of wave energy harvesting [5], as well as several prototypes already installed along the Chilean coast [6].

The diversity of the wave resources and the instability of energy intensity make the design of wave energy converter systems (WECs) very challenging [7,8]. To overcome these difficulties, selecting technologies for generating electrical energy from capturing mechanical energy is a crucial aspect of the design [9]. In this regard, the combination of point absorbers, which harvest the energy from the motion of submerged or floating buoys [10], and linear generators, which provide high energy density and direct conversion [11], have proved to be highly efficient because the mechanical swinging movement is directly transformed into electrical energy. Several examples of linear generators used with point absorbers have been reported, such as the Seacap (France), Islandberg Project (Sweden), PowerBouy (New Jersey), InfinityWEC (Sweden), PowerPod (UK), among others [12].



Citation: Zapata, H.M.; Perez, M.A.; Marquez Alcaide, A. Control of cascaded multilevel converter for wave energy applications. *Energies* **2023**, *16*, 71. <https://doi.org/10.3390/en16010071>

Academic Editor: Adolfo Dannier

Received: 9 November 2022

Revised: 13 December 2022

Accepted: 15 December 2022

Published: 21 December 2022



Copyright: © 2022 by the authors. Licensee MDPI, Basel, Switzerland. This article is an open access article distributed under the terms and conditions of the Creative Commons Attribution (CC BY) license (<https://creativecommons.org/licenses/by/4.0/>).

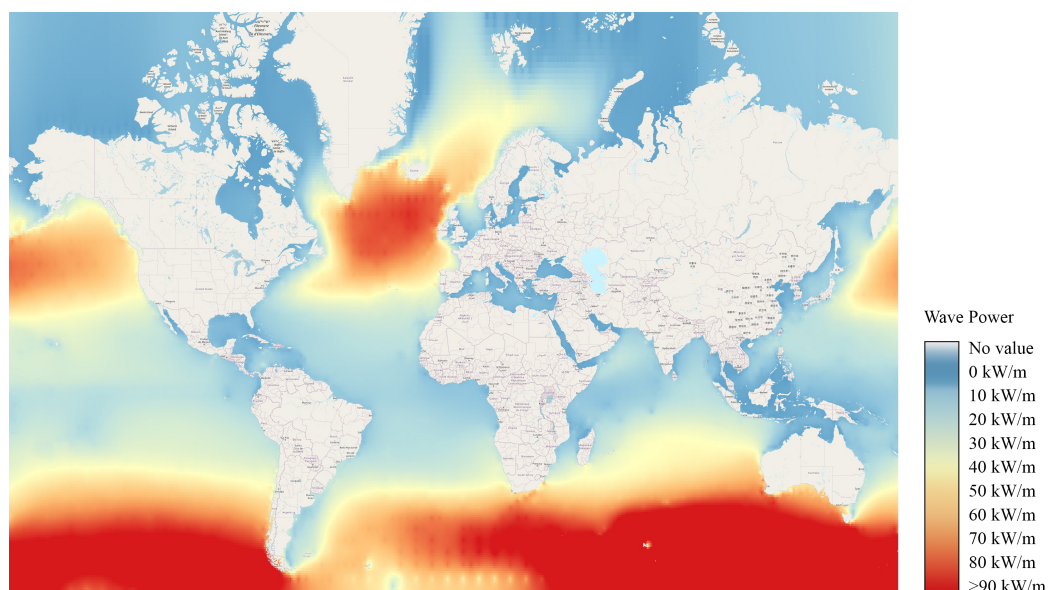


Figure 1. World map of wave power (obtained from [13]).

Linear generators offer a simple and robust structure for electromagnetic conversion of a swinging movement [14]. A tubular permanent magnet linear generator (TPMLG) is a typical choice to harvest wave energy efficiently, and some shapes of permanent magnets (PMs) can optimize their properties, such as increasing flux linkage, reducing cogging force, or improving conversion efficiency [15,16]. The PMs can be oriented using radial, axial, or Halbach configurations to modify the magnetic flux path for different translator-stator combinations [17]. The PMs are usually located in the translator, while a modular arrangement of the windings in the stator is usually employed to bring flexibility for easy sizing [18].

The power extracted from the waves depends on the operating frequency and is maximized when the frequency of the WEC matches the wave frequency [19]. There are several control strategies focused on extracting the maximum power from the wave, which can be classified depending on whether the control action to achieve resonance is imposed on the mechanical elements or the electromagnetic devices [20]. The search for the appropriate operating frequency is very challenging due to the irregular period and amplitude of the waves. The wave period can be estimated using the velocity and acceleration information, but additional mechanical sensors are required for a precise estimation [21]. A passivity-based approach in which the velocity is associated with the wave energy can also be used to maximize the extracted energy [22]. On the other hand, a Hill-climbing algorithm, in which the electrical variables are slightly modified, and according to the power variation, the best operating condition is selected, provides good tracking performance without using additional sensors [23]. Multilevel converters based on submodules, such as the cascaded H-bridge and modular multilevel converter, allow the linear generator windings to be connected to different submodules, further increasing the energy harvesting by using separated Maximum Power Point Tracking (MPPT) [24].

High-voltage direct current (HVDC) and Medium Voltage Direct Current (MVDC) technologies are particularly well suited for submarine power transmission due to the reduced losses, no requirements for reactive power compensation, and lower costs than AC transmission [25,26]. Multilevel converters produce higher voltages than two-level converters, generating a voltage waveform composed of several voltage levels [27], reaching MVDC and HVDC operation voltages [28]. Due to the high-quality waveforms, they do not require filters; hence, the power density is increased. This power density is a critical parameter in wave energy conversion systems due to the limited space inside the buoy [29].

This paper presents a wave energy converter based on a linear generator, a multilevel cascaded converter, and its control scheme. Each generator winding is connected to a

submodule of the converter and controlled independently to operate at the maximum power point. The control loop at the input side of the submodule maximizes the extracted power from the linear generator and due to the independent connection of each submodule, the extracted power could be different leading to the unbalances of the capacitor voltages. A second control loop at the output side of the submodule is proposed to balance the capacitor voltages and generate the output voltage. Both controllers are tested experimentally demonstrating their performance.

2. Wave Energy Conversion System

A wave energy conversion system uses three energy conversion stages to extract the mechanical energy, transform it, and inject it into the electrical grid. As shown in Figure 2, a buoy works as a point absorber mechanism that uses the action of the incident sea waves to move the linear generator translator up and down without gears, levers, or any other additional mechanical system. A mooring system is used to keep the buoy and WEC system stationary. The cascaded multilevel power converter takes the energy from the linear generator and transforms it into a medium voltage signal which transmits the energy to the coast employing a transmission cable. At the coast, a second power converter receives the energy from the WEC and transforms it into a three-phase voltage, injecting it into the grid. An arrangement of buoys can be installed in a given area connecting them to the same onshore converter.

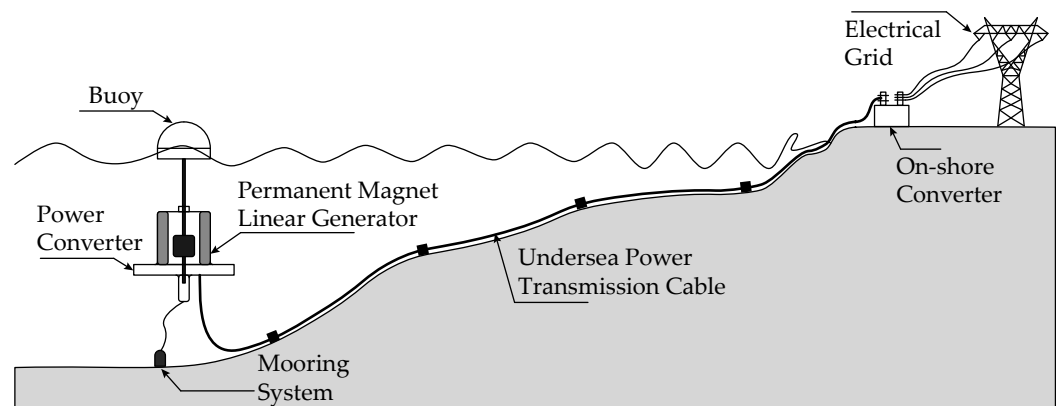


Figure 2. Wave energy converter system.

2.1. Linear Generator

The linear generator is implemented with a tubular shape, divided into two structures: the translator and the stator. The translator is mounted on a mobile vertical shaft attached to the buoy, as shown in Figure 3. The translator has ring-shaped PMs, which have an axial configuration being the north orientation pointed to the outer side. The stator has a tubular shape and supports the coils arranged around it. Each coil is connected independently to a submodule of the power converter. When the translator moves, the PMs induce voltages in the coils, and the power converter is controlled to extract the generated power. A detailed analysis of the linear generator analysis and design, including the flux equations and finite element analysis, is given in [29].

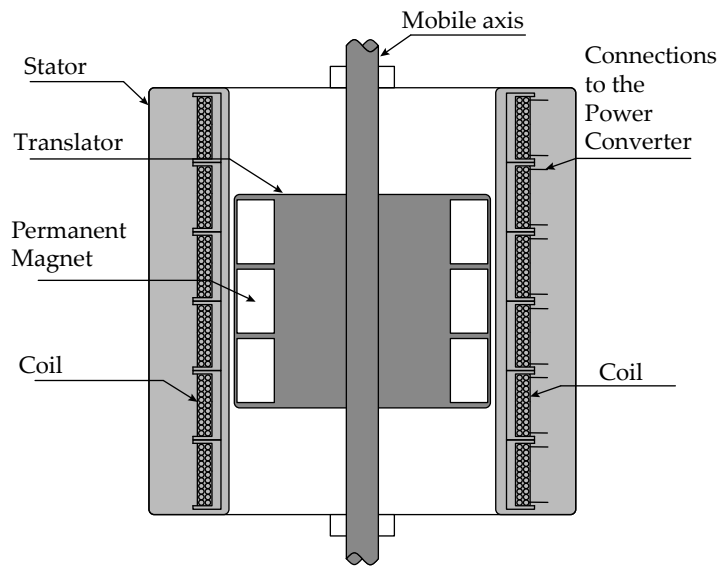


Figure 3. Tubular permanent magnet linear generator.

2.2. Power Converter

A cascaded converter is used to harvest energy from the linear generator. As shown in Figure 4, each coil is connected independently to a power converter submodule, and the outputs of all submodules are connected in series to generate a medium voltage which is applied to the submarine transmission line. At the onshore side of the line, another converter is connected, which transforms the DC voltages and currents into three-phase signals to inject the power into the electrical grid.

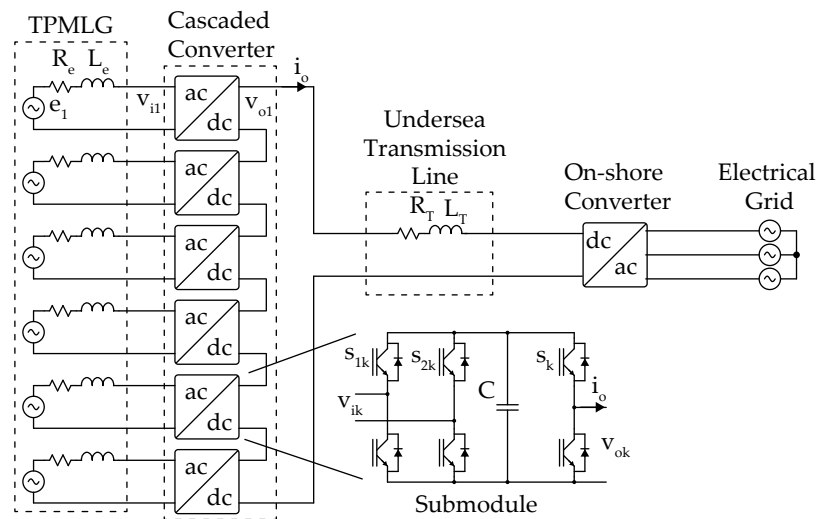


Figure 4. Cascaded inverter and grid connection.

Each submodule is composed of a full-bridge AC-DC converter, a DC capacitor, and a half-bridge DC-DC converter, as shown in Figure 4. The full-bridge converter is used to control the current taken from the generator by using an MPPT algorithm, while the half-bridge converter is used to keep the capacitor voltage at its reference level, transferring the power to the line.

3. Proposed Control System

The control system is composed by two stages, as shown in Figure 5. The first stage manages the full-bridge converter using an MPPT algorithm which generates the current reference to extract the maximum power from the linear generator winding and inject it into

the DC capacitor. The second stage manages the half-bridge to extract the energy from the DC capacitor keeping its voltage controlled and generating the DC voltage for MVDC transmission.

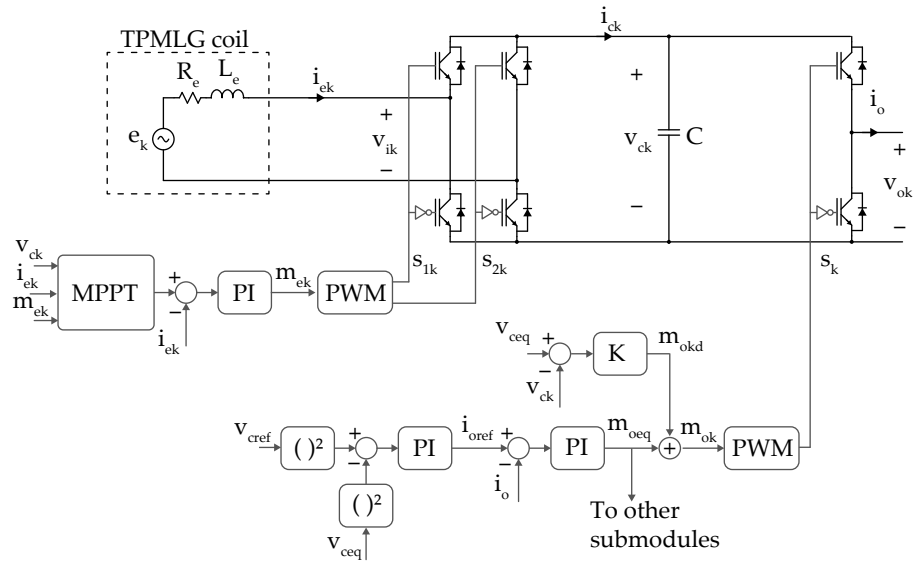


Figure 5. Control scheme of a submodule.

3.1. Full-Bridge Control

The MPPT algorithm determines the current reference for the AC-DC stage to maximize the power extracted from each coil. The proposed MPPT algorithm is based on the nature of the frequency of the waves and the electrical system measurements.

Considering a linear model of the windings, as shown in Figure 5, for a given harmonic ω_e , the input voltage can be calculated as

$$v_{ik} = e_k - (R_e + j\omega_e L_e)i_{ek} \tag{1}$$

The active power at the converter terminals can be calculated as

$$P = \Re\{v_{ik}i_{ek}^*\} \tag{2}$$

Calculating from the previous equations the current which generates the maximum active power results in

$$I_{ekd} = \frac{E_{kd}}{2R_e} \tag{3}$$

$$I_{ekq} = \frac{E_{kq}}{2R_e} \tag{4}$$

where $I_{ek} = I_{ekd} + jI_{ekq}$ and $E_k = E_{kd} + jE_{kq}$ are the direct and quadrature components of the input current and induced voltage phasors, respectively. From the previous result, it is possible to notice that to obtain the maximum active power, the current must be in-phase with the induced voltage. Repeating the previous analysis but solving for the converter voltage results in

$$V_{ikd} = \frac{E_{kd}}{2} - \frac{\omega_e L_e}{R_e} \frac{E_{kq}}{2} \tag{5}$$

$$V_{ikq} = \frac{E_{kq}}{2} + \frac{\omega_e L_e}{R_e} \frac{E_{kd}}{2} \tag{6}$$

where $V_{ik} = V_{ikd} + jV_{ikq}$ (components in coordinates dq) is the converter input voltage phasor. Therefore, the voltage at the converter terminals is a combination of the direct and quadrature component of the induced voltage at a given frequency.

It is impossible to directly obtain the voltage or current reference because the induced voltage cannot be measured. This paper employs a perturb-and-observe algorithm by measuring the current, capacitor voltage, and modulation index and generating a reference for the input current according to the calculated power; the values of L_t and R were considering that the transmission line should reach the on-shore converter. The values of L_e and R_e used were approximated from the data of a linear generator from Gieras [30].

The model of the input current in terms of the modulation index in the domain of frequency “ s ” is

$$I_{ek}(s) = \frac{-V_{ck}M_{ek}(s)}{L_e s + R_e} \quad (7)$$

where I_{ek} is the coil current, M_{ek} is the modulation index for the converter, V_{ck} is the capacitor voltage, R_e is the coil resistance, and L_e is coil inductance. Once the current reference is obtained, a PI controller is employed to generate the modulation index. This controller is designed by pole placement using the previous equation and adjusting the response time to 5 ms. Table 1 shows the system parameters used to design the controllers.

Table 1. Parameters of the WEC system.

Parameter	Value
Coil Inductance (L_e)	15 mH
Coil Resistance (R_e)	1 Ω
DC capacitance (C)	2.200 μ F
Line Inductance (L_T)	20 mH
Equivalent system resistance (R)	10 Ω

After the PI controller generates the modulation signal, a bipolar Pulse-width modulation (PWM) is employed to generate the switching signals for the full-bridge converter.

3.2. Half-Bridge Control

The main control objective of the half-bridge control scheme is to transfer the power from the DC-link to the output terminals and to keep the capacitor voltages balanced at a given level.

Each winding generates a different amount of power which is transferred from the input terminals to the output terminals of the submodule. The output current is the same for all submodules, hence the output voltage must differ. Considering the capacitor voltages controlled at the same value, the modulation indexes for each submodule must also be different.

To manage the power transferred in all the submodules, the control system is composed of a mean component controller and a differential component controller, which are analyzed below.

The total output voltage is defined by

$$v_o = \sum_{k=1}^N v_{ok} = \sum_{k=1}^N v_{dck} m_{ok} \quad (8)$$

Considering both, the capacitor voltages and the modulation indexes, different in each submodule, this voltage can be written as

$$v_o = \sum_{k=1}^N (v_{dceq} + v_{dckd})(m_{oeq} + m_{okd}) \quad (9)$$

where v_{dceq} and m_{oeq} are the mean values of the capacitor voltage and modulation index, respectively, and v_{dcd} and m_{okd} are the differential components of the capacitor voltage and modulation index, respectively. Defining the mean value as

$$v_{dceq} = \frac{1}{N} \sum_{k=1}^N v_{dck} \quad m_{oeq} = \frac{1}{N} \sum_{k=1}^N m_{ok} \quad (10)$$

results in

$$\sum_{k=1}^N v_{dckd} = \sum_{k=1}^N m_{okd} = 0 \quad (11)$$

Replacing the output voltage definition and neglecting the product of differentials results in

$$v_o = Nv_{dceq}m_{oeq} + v_{dceq} \sum_{k=1}^N m_{okd} + m_{oeq} \sum_{k=1}^N v_{dckd} + \sum_{k=1}^N v_{dckd}m_{okd} = Nv_{dceq}m_{oeq} \quad (12)$$

Therefore the total output voltage, and hence the output current, is given by the mean value of the modulation index.

Considering an inductive-resistive load to model the transmission line, the onshore converter and the electrical system, the dynamical equation is given by

$$L_T \frac{di_o}{dt} + Ri_o = Nv_{dceq}m_{oeq} \quad (13)$$

The mean current PI controller is designed using the previous equation by the pole placement technique adjusting a response time of 5 ms.

In each capacitor, the voltage is given by the following dynamical equation

$$C \frac{dv_{dck}}{dt} = m_{ek}i_{ek} - m_{ok}i_o \quad (14)$$

where i_o is the output current, m_{ok} is the modulation index for the half-bridge, m_{ek} and i_{ek} are the modulation index and current in the full-bridge, and C is the capacitance. The current coming from the full-bridge is considered a disturbance of the system, so it is neglected. Calculating the mean capacitor voltage results in

$$C \frac{dv_{dceq}}{dt} = - \sum_{k=1}^N (m_{oeq} + m_{okd})i_o = -m_{oeq}i_o \quad (15)$$

Multiplying by the mean voltage to obtain the power and considering a constant line voltage V_L imposed by the onshore converter, the model results in

$$\frac{C}{2} \frac{dv_{dceq}^2}{dt} = -V_L i_o \quad (16)$$

Therefore, to increase the energy in the capacitor (i.e., the square of the capacitor voltage), the output current must be reduced and vice versa. Using this dynamical model, a PI controller for the output current using the pole placement technique is designed adjusting the response time to 50 ms.

Once the output current is controlled, Equation (14) can be written in terms of the differential values as

$$C \frac{dv_{dckd}}{dt} = -m_{okd}i_o \quad (17)$$

Considering this expression, the relation between the differential voltage capacitor and the differential modulation index is an integral, and hence, a proportional term K can be used for control, as shown in Figure 5.

The modulation index of each submodule composed of the mean and differential values is modulated using PWM to generate the gating signals for the half-bridge converter.

4. Experimental Results

An experimental setup is built to verify the proposed control scheme. The setup is shown in Figure 6, where it is possible to identify the submodules of the cascaded converter. The experimental setup is composed of three submodules, each connected to the secondary of a transformer whose input signal emulates the induced electromotive force (EMF) obtained in [29]. The output of the submodules is connected in series to an inductance and a resistance which model the underwater transmission line. Although the proposed cascaded multilevel converter is intended to generate medium voltage by using ten cells of 500 V each, the experimental setup is limited to three cells due to the limited availability of converters to emulate the linear generator. The DC voltage of each cell is also reduced to 35 V for safety purposes.

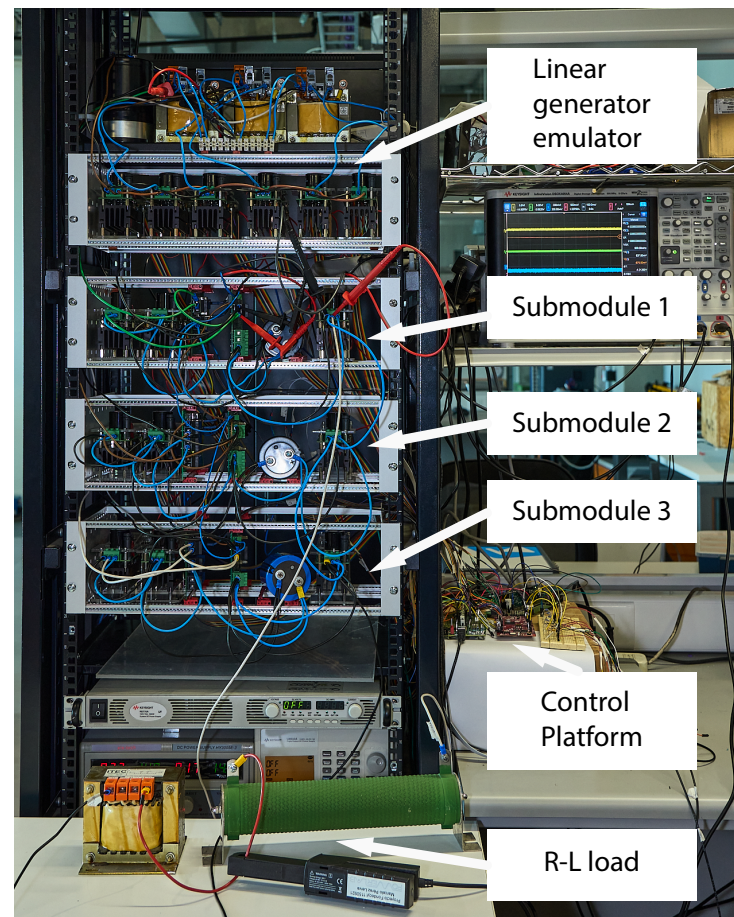


Figure 6. Picture of the experimental setup.

The control platform is based on two Texas Instruments (TI) Delfino boards. One board is used to control the linear generator emulator and another board is employed to control the three submodules. The following results show the behavior of each submodule identified by the yellow, green, and blue colors, corresponding to submodules 1, 2, and 3, respectively.

Figure 7a shows the EMF voltages obtained from the linear generator emulator. The wave frequency was set to 1 Hz, and the height of the coils was defined as equal to the

height of PMs. The translator is set to move between the first and the third coil; hence, no blank times without any induced voltage are generated.

Figure 7b shows the current extracted from the coils. The MPPT algorithm generates the reference of this current. It is possible to notice that the current waveform resembles the induced EMF, as the analysis has shown.

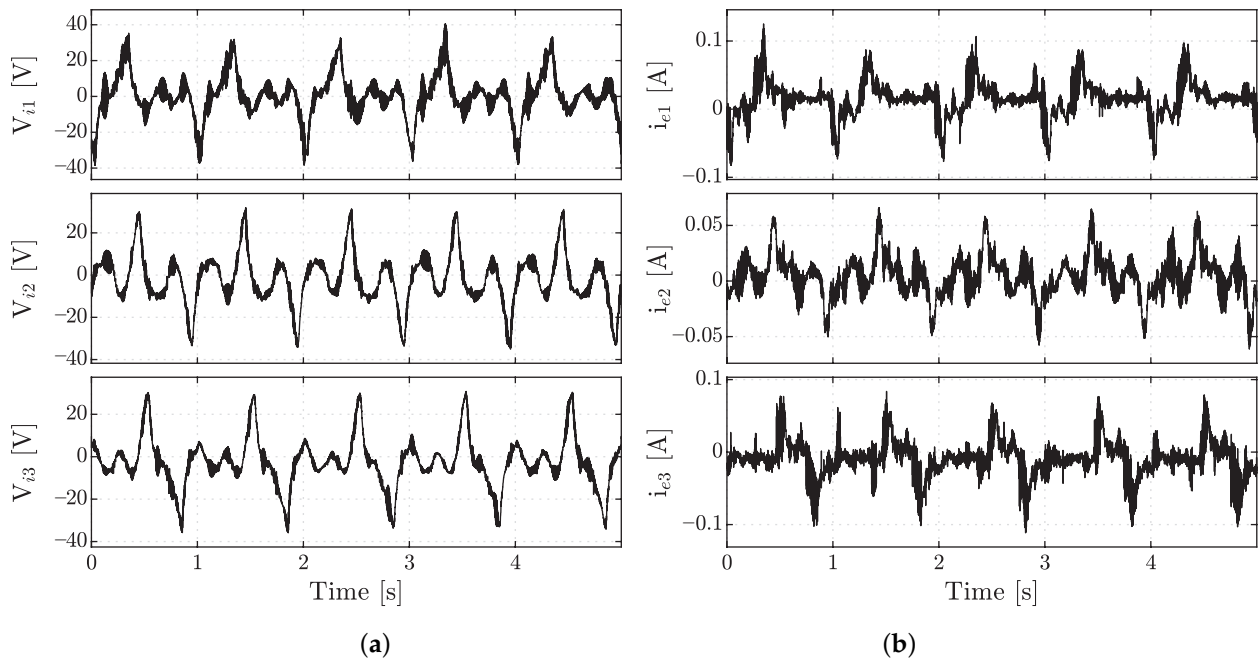


Figure 7. Experimental results. (a) Induced EMF. (b) Input submodule current.

Figure 8a shows the current flowing from the full-bridge converter to the capacitor. This current, as the capacitor voltage can be considered constant, resembles the power extracted from the coils of the linear generator.

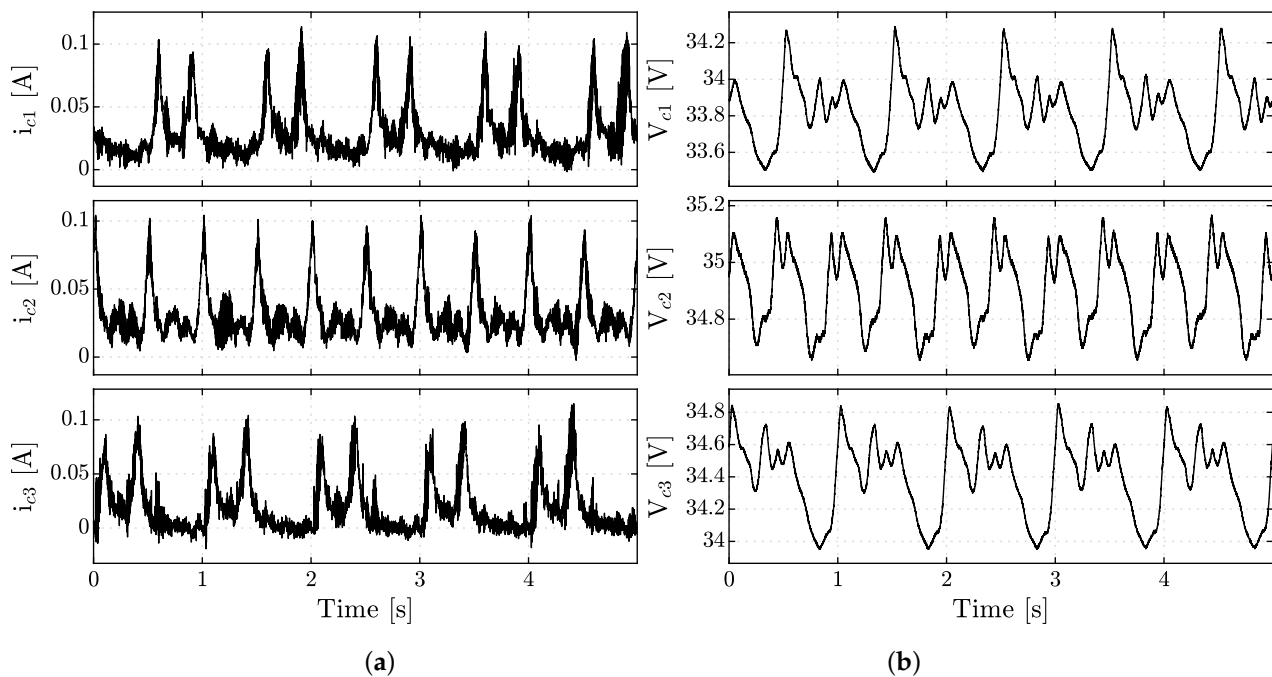


Figure 8. Experimental results. (a) Current flowing from the full-bridge to the capacitor (b) DC-link capacitor voltages.

Figure 8b shows the capacitor voltages. The mean value is set to 35 V, and the difference between them is less than 1 V.

Figure 9a shows the output current in pink color. This current is the combination of the power injected by the three modules; hence, it resembles the total power extracted from the linear generator.

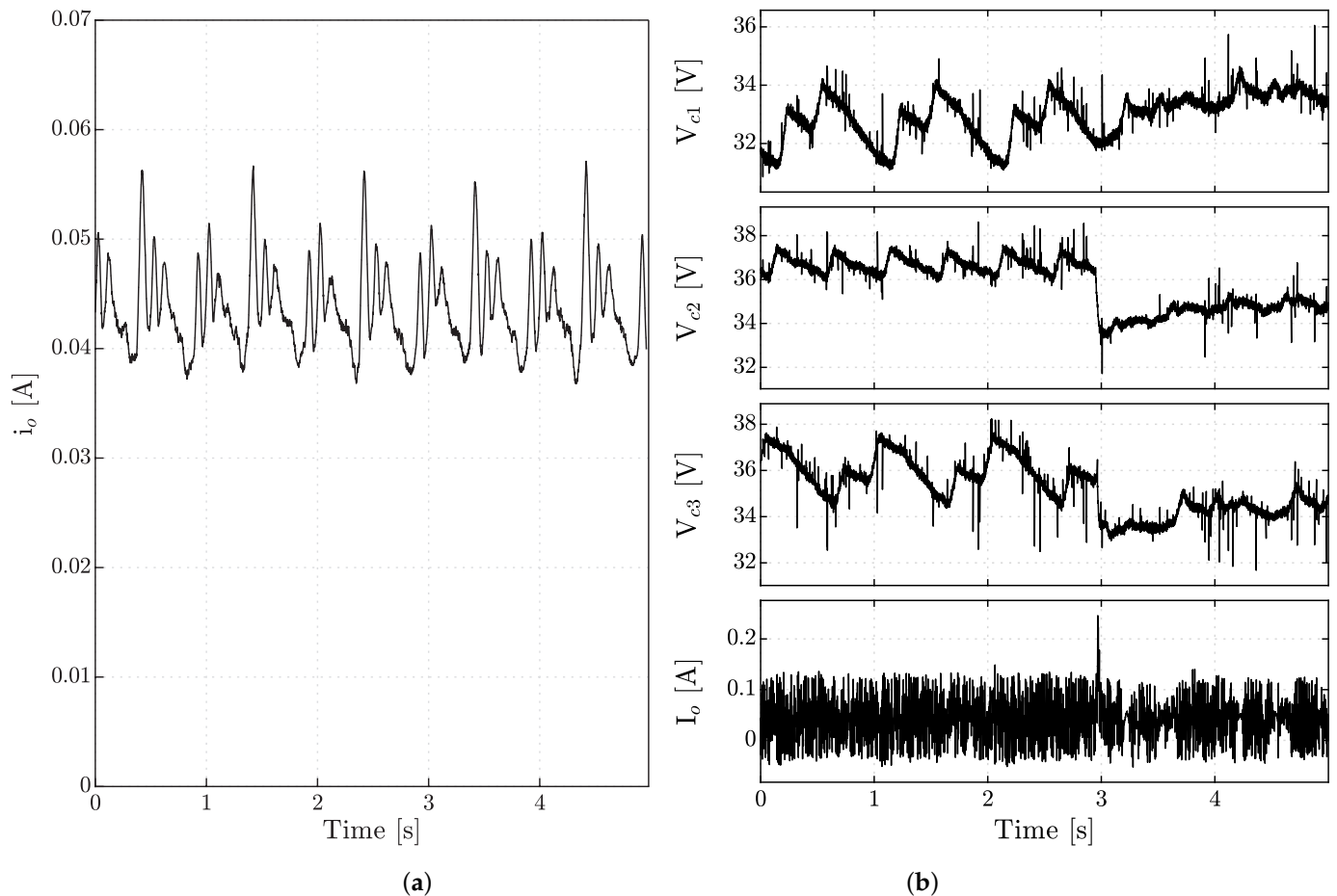


Figure 9. Experimental results. (a) Output current; (b) performance of the capacitor balance strategy.

Figure 9b shows the activation of the voltage balancing loop. It is possible to notice that the voltages of the three capacitors are separated first, and they are balanced when the balancing loop is activated. There is a commercial model of WEC with an output voltage of 24 to 300 volts and a peak load power of 3 kW; our results have been designed to have an output voltage of 35 V and a peak current of 200 mA.

The power generated by direct conversion WECs, such as the proposed in this paper, has a large variation due to the reduction of speed at the top and bottom of the linear generator. This effect is shown in Figure 8 in the DC-link currents. However, it can be minimized by adding storage in the on-shore converter [31]. This converter is out of the scope of this paper.

5. Conclusions

A WECs system is shown in this paper, which uses a buoy as a point absorber and a linear generator as a power take-off device. The linear generator has independent coils, which are powered sequentially as the translator moves up and down. A cascaded converter is employed to drive the linear generator connecting each winding to its respective converter submodule. The output of the submodules is connected in series to generate a medium voltage to the transmission line.

The proposed control scheme is based on two stages: an MPPT algorithm to extract the power from the linear generator and transfer it to the DC capacitor and a DC capacitor controller to transfer the power from the capacitor to the transmission line. Experimental results show the performance of the controller, which allows for optimization of the energy extracted, balancing capacitor voltages, and power injection to the system.

Author Contributions: Conceptualization, M.A.P. and H.M.Z.; methodology, M.A.P.; software, H.M.Z.; validation, H.M.Z. and M.A.P.; formal analysis, H.M.Z.; investigation, H.M.Z.; resources, M.A.P.; data curation, H.M.Z.; writing—original draft preparation, H.M.Z.; writing—review and editing, H.M.Z., M.A.P. and A.M.A.; visualization, H.M.Z.; supervision, M.A.P.; project administration, M.A.P.; funding acquisition, M.A.P. All authors have read and agreed to the published version of the manuscript.

Funding: This research was funded by the Advanced Center for Electrical and Electronics Engineering(AC3E) under Grant ANID/FB0008, by the Solar Energy Research Center (SERC) under Grant ANID/FONDAP/15110019, by the ANID/Fondecyt Regular Grant 1211826, and by ANID+Doctorado Nacional 2020+21200544.

Data Availability Statement: Not applicable

Conflicts of Interest: The authors declare no conflict of interest.

References

1. REN21. *Renewables 2021 Global Status Report*; Technical Report, Renewable Energy Policy Network for the 21st Century; REN21 Secretariat: Paris, France, 2021. Available online: <https://www.ren21.net/reports/global-status-report/> (accessed on 19 December 2022).
2. International Renewable Energy Agency (IRENA). *Renewable Capacity Statistics*. Available online: <https://www.irena.org/publications/2021/March/Renewable-Capacity-Statistics-2021> (accessed on 19 December 2022).
3. Gunn, K.; Stock-Williams, C. Quantifying the global wave power resource. *Renew. Energy* **2012**, *44*, 296–304. [CrossRef]
4. Ulazia, A.; Penalba, M.; Rabanal, A.; Ibarra-Berastegi, G.; Ringwood, J.; Sáenz, J. Historical Evolution of the Wave Resource and Energy Production off the Chilean Coast over the 20th Century. *Energies* **2018**, *11*, 2289. [CrossRef]
5. Aquatera Ltd. *Recommendations for Chile's Marine Energy Strategy: A Roadmap for Development*; Foreign and Commonwealth Office: 2014; Available online: <https://www.gov.uk/government/publications/recommendations-for-chiles-marine-energy-strategy> (accessed on 19 December 2022).
6. Khan, M.Z.A.; Khan, H.A.; Aziz, M. Harvesting Energy from Ocean: Technologies and Perspectives. *Energies* **2022**, *15*, 3456. [CrossRef]
7. Drew, B.; Plummer, A.R.; Sahinkaya, M.N. *A Review of Wave Energy Converter Technology*; Sage Publications Sage: London, UK, 2009.
8. Czech, B.; Bauer, P. Wave Energy Converter Concepts: Design Challenges and Classification. *IEEE Ind. Electron. Mag.* **2012**, *6*, 4–16. [CrossRef]
9. Aderinto, T.; Li, H. Review on Power Performance and Efficiency of Wave Energy Converters. *Energies* **2019**, *12*, 4329. [CrossRef]
10. Melikoglu, M. Current status and future of ocean energy sources: A global review. *Ocean. Eng.* **2018**, *148*, 563–573. [CrossRef]
11. Aamir Hussain Memon, B.; Ibrahim, T.; Perumal, N. Portable and pico-scale linear generator for wave energy conversion. In Proceedings of the 5th International Conference on Intelligent and Advanced Systems (ICIAS), Kuala Lumpur, Malaysia, 3–5 June 2014; pp. 1–4.
12. Wave Devices: EMEC: European Marine Energy Centre. Available online: <http://www.emec.org.uk/marine-energy/wave-devices/> (accessed on 19 December 2022).
13. System Web GIS: OES: Ocean Energy System. Available online: <https://www.ocean-energy-systems.org/ocean-energy/gis-map-tool/> (accessed on 19 December 2022).
14. Wang, J.; Jewell, G.W.; Howe, D. A general framework for the analysis and design of tubular linear permanent magnet machines. *IEEE Trans. Magn.* **1999**, *35*, 1986–2000. [CrossRef]
15. Abdalla, I.I.; Ibrahim, T.; Nor, N.M. Analysis of Tubular Linear Motors for Different Shapes of Magnets. *IEEE Access* **2018**, *6*, 10297–10310. [CrossRef]
16. Curcic, M.; Quaicoe, J.E.; Bachmayer, R. A novel double-sided linear generator for wave energy conversion. In Proceedings of the OCEANS 2015, Genova, Italy, 18–21 May 2015; pp. 1–7.
17. Mesantono, L.D.; Danang Wijaya, F.; Haryono, T. Comparison of linear flux permanent magnet generator topologies by using FEMM 2D. In Proceedings of the 8th International Conference on Information Technology and Electrical Engineering (ICITEE), Yogyakarta, Indonesia, 5–6 October 2016; pp. 1–5.
18. Hodgins, N.; Keysan, O.; McDonald, A.S.; Mueller, M.A. Design and Testing of a Linear Generator for Wave-Energy Applications. *IEEE Trans. Ind. Electron.* **2012**, *59*, 2094–2103. [CrossRef]

19. Maria-Arenas, A.; Garrido, A.J.; Rusu, E.; Garrido, I. Control Strategies Applied to Wave Energy Converters: State of the Art. *Energies* **2019**, *12*, 3115. [[CrossRef](#)]
20. Wang, J.; Chen, Z.; Zhang, F. A Review of the Optimization Design and Control for Ocean Wave Power Generation Systems. *Energies* **2022**, *15*, 102. [[CrossRef](#)]
21. Park, J.S.; Gu, B.G.; Kim, J.R.; Cho, I.H.; Jeong, I.; Lee, J. Active Phase Control for Maximum Power Point Tracking of a Linear Wave Generator. *IEEE Trans. Power Electron.* **2017**, *32*, 7651–7662. [[CrossRef](#)]
22. Huang, W.; Yang, J. A Novel Piecewise Velocity Control Method Using Passivity-Based Controller for Wave Energy Conversion. *IEEE Access* **2020**, *8*, 59029–59043. [[CrossRef](#)]
23. Xiao, X.; Huang, X.; Kang, Q. A Hill-Climbing-Method-Based Maximum-Power-Point-Tracking Strategy for Direct-Drive Wave Energy Converters. *IEEE Trans. Ind. Electron.* **2016**, *63*, 257–267. [[CrossRef](#)]
24. Perez, M.A.; Bernet, S.; Rodriguez, J.; Kouro, S.; Lizana, R. Circuit Topologies, Modeling, Control Schemes, and Applications of Modular Multilevel Converters. *IEEE Trans. Power Electron.* **2015**, *30*, 4–17. [[CrossRef](#)]
25. Páez, J.D.; Frey, D.; Maneiro, J.; Bacha, S.; Dworakowski, P. Overview of DC–DC Converters Dedicated to HVdc Grids. *IEEE Trans. Power Deliv.* **2019**, *34*, 119–128. [[CrossRef](#)]
26. Han, X.; Sima, W.; Yang, M.; Li, L.; Yuan, T.; Si, Y. Transient Characteristics Under Ground and Short-Circuit Faults in a ± 500 kV MMC-Based HVDC System With Hybrid DC Circuit Breakers. *IEEE Trans. Power Deliv.* **2018**, *33*, 1378–1387. [[CrossRef](#)]
27. Monopoli, V.G.; Marquez, A.; Leon, J.I.; Liserre, M.; Buticchi, G.; Franquelo, L.G.; Vazquez, S. Applications and Modulation Methods for Modular Converters Enabling Unequal Cell Power Sharing: Carrier Variable-Angle Phase-Displacement Modulation Methods. *IEEE Ind. Electron. Mag.* **2022**, *16*, 19–30. [[CrossRef](#)]
28. Müller, N.; Kouro, S.; Malinowski, M.; Rojas, C.A.; Jasinski, M.; Estay, G. Medium-Voltage Power Converter Interface for Multigenerator Marine Energy Conversion Systems. *IEEE Trans. Ind. Electron.* **2017**, *64*, 1061–1070. [[CrossRef](#)]
29. Zapata, H.M.; Pérez, M.A. Modular Multilevel Converter for a Linear Generator for Wave Energy Converter. *Energies* **2022**, *15*, 6346. [[CrossRef](#)]
30. Gieras, J.F.; Piech, Z.J.; Tomczuk, B. *Linear Synchronous Motors: Transportation and Automation Systems*; CRC Press: Boca Raton, FL, USA, 2016.
31. Rasool, S.; Islam, M.R.; Muttaqi, K.M.; Sutanto, D. An Advanced Control Strategy for a Smooth Integration of Linear Generator Based Wave Energy Conversion System with Distribution Power Grids. In Proceedings of the 2019 IEEE Industry Applications Society Annual Meeting, Baltimore, MD, USA, 29 September–3 October 2019; pp. 1–6. [[CrossRef](#)]

Disclaimer/Publisher’s Note: The statements, opinions and data contained in all publications are solely those of the individual author(s) and contributor(s) and not of MDPI and/or the editor(s). MDPI and/or the editor(s) disclaim responsibility for any injury to people or property resulting from any ideas, methods, instructions or products referred to in the content.